

Percolation Effect Induced Significant Change of Complex Permittivity and Permeability for Silver-Epoxy Nano-Composites

Bo-Wei Tseng and Tsun-Hsu Chang*

Department of Physics, National Tsing Hua University, Hsinchu 30013, Taiwan

The intricate interplay between complex permittivity and permeability constitutes the cornerstone of electromagnetic (EM) applications, enabling precise customization for various uses. This study employed silver-epoxy nano-composites to exemplify a conductor-insulator composite, leveraging silver's exceptional attributes, such as high conductivity and low reactivity. The determination of complex permittivity and permeability was conducted via the transmission/reflection method. At lower concentrations of dispersed silver particles, these nano-particles within the epoxy resin act as modest dipoles, augmenting permittivity. This regime aligns closely with the effective medium theory (EMT) and comprises the focus of much research. However, nearing the percolation threshold, a percolation effect emerges, drastically accelerating enhancement rates beyond the predictions of EMT. Simultaneously, long-wavelength electromagnetic waves induce diamagnetic currents within loops formed by metal grains. This diamagnetic effect intensifies with increasing volume fraction, leading to a reduction in permeability. This study observed percolation power law behavior near the threshold with calculated critical exponents. Consequently, the dielectric constant of the silver-epoxy nano-composite reached a maximum of 515. Regarding the relative permeability, the lowest recorded value was 0.31. These findings were obtained within the X-band (8.2 GHz~12.4 GHz) region.

*Electronic mail: thschang@phys.nthu.edu.tw

Metamaterial and composite material have grab attention in recent years, since it can possess unique properties that don't exist in the nature [1-5]. Investigating the EM properties enable us to fine tune the EM properties for specific use. The most common analysis method for composites is the effective medium theory (EMT). However, its efficacy diminishes when the volume fraction is tuned widely, due to the lack of prediction in threshold. Yao *et al.* have collected the ten most representative EMT models [6], all of which can only handle a small region in volume fraction, and none of those predicted a threshold. Also, EMT is limited in dielectric constant ($\epsilon_0\epsilon'$). EMT cannot explain the imaginary part ($\epsilon_0\epsilon''$) and the complex permeability ($\mu_0\mu' + i\mu_0\mu''$). This is where the percolation theory kicks in.

The percolation theory was first introduced in 1957 by Boardbent and Hammersley [7]. Most of the investigation in the last six decades focus on the dielectric constant (ϵ') and the electrical conductivity (σ). To the authors' best knowledge the research of ϵ'' [8] and $\mu' + i\mu''$ [9-11] stopped after 1990s. This is due to the lack of application. However, this doesn't mean that the properties are not important, since EM wave consists of both permittivity and permeability, and they are usually mixed with each other (etc. refraction index and wave impedance). If the permeability is just 1, this won't be a problem. Nevertheless, when one deals with composites or metamaterials, one can't just naively suggest permeability to be 1. Su *et al.* showed that silver-epoxy composite exhibits diamagnetism while epoxy and silver are both non-magnetism [12]. Lagar'kov *et al.* showed that the permeability of ferromagnetic percolation system also has diamagnetic percolative behavior [11]. Bowman and Stroud showed that superconductor-metal composites also possess diamagnetism and follow the percolation power law [10]. They also predicted that metal-insulator composites also have similar properties. Therefore, magnetism may not be rare in composites, and if one naively makes permeability 1, one may result in a wrong permittivity.

The behavior of a composite's dielectric constant is studied [13-15]. It reads

$$\epsilon' = \begin{cases} \epsilon_d' |p - p_c|^{-s} & p < p_c, p > p_c \\ \epsilon_d' \frac{t}{t+s} \left(\frac{\sigma_m}{\omega}\right)^{\frac{s}{t+s}} & p \text{ near } p_c \end{cases} \quad (1a)$$

$$(1b)$$

p is the volume fraction, p_c is the percolation threshold; ϵ_d' is the dielectric constant of the insulator; σ_m is the conductivity of the metal, and s as well as t are the critical exponents. The theoretical value is 0.7~1.0 for s in 3D. Near the threshold, there is a remarkable surge in the

dielectric constant, reaching a tremendously significant value. However, this substantial enhancement is confined to a narrow vicinity. Consequently, accurately calculating the volume fraction near the threshold poses a challenging task. The imaginary part also follows the power law [8]

$$\varepsilon'' \propto \begin{cases} |p - p_c|^{-q} & p < p_c \\ \left(\frac{\sigma_m}{\omega}\right)^{\frac{s}{t+s}} & p \text{ near } p_c \end{cases} \quad (2a)$$

$$(2b)$$

The critical exponent q has a theoretical value of 2.5~3.1 in 3D.

According to Bowman's model, long-wavelength electromagnetic waves induce diamagnetic currents in loops formed by metal grains. This diamagnetic effect intensifies with an increase in volume fraction, causing a reduction in permeability due to the more fabulous presence of "bond" electrons. However, as the volume fraction continues to rise, the swift expansion of silver nanoparticle clusters prompts the 'bond' electrons to transition back to a 'free' state. Consequently, the induced current weakens, leading to an increase in permeability. The negative magnetic susceptibility ($-\chi_b$) follows the power law near the threshold [9,10]

$$-\chi_b \propto |p - p_c|^{-u} \quad p \text{ close to } p_c \quad (3)$$

The critical exponent u for the negative magnetic susceptibility has the theoretical value about 0.11~0.41 [10]. As for the imaginary part, it reads[10,11]

$$\mu'' \propto |p - p_c|^{-v} \quad p \text{ close to } p_c \quad (4)$$

The critical exponent v also has a theoretical value equal to u [10].

Our sample preparation closely followed the established waveguide method [16]. The WR90 (X-band) waveguide went through a washing process first, then be affixed to the Teflon holder. The holder comprised five components: a metal base, two WR90-shaped Teflon plates, and two Teflon plates. Structurally resembling a sandwich, the holder featured the metal base at the bottom, followed by a plate, with the WR90-shaped plates flanking the copper waveguide. Before sealing

the waveguide, the composite mixture was introduced. The nano-powder utilized in this study was commercially sourced from US Research Nanomaterials, Inc., boasting a purity exceeding 99.99%, a diameter of 20 nm, and a density of 10.49 g/cm³. The epoxy resin (Epoxy A) employed possessed notable adhesive properties. When combined with the hardener (Epoxy B), the epoxy exhibited a density of about 1.13 g/cm³.

The fabrication began by pouring one to three grams of Epoxy A into a flask, then the desired volume fraction of powder was added, and a moderate stirring ensued. Once the mixture achieved homogeneity, Epoxy B was introduced. The resulting composite was then poured into the Teflon holder, sealed with the final round plate, and secured with screws. The holder was placed in a custom-made oven capable of reaching temperatures around 80 °C to expedite curing. The metal base, designed to be affixed to a motor inside the oven, provided the sample with a moderate rotation during curing, preventing nano-particle precipitation. Elevating the temperature to 70-90 °C allowed the composite to harden within 3 hours. Upon completion of curing, the composite underwent a polishing phase. The desired outcome was a smooth surface for the composite, devoid of any cavities, pores, or holes to ensure the acquisition of precise results. The fabrication process of the composite is illustrated in [Fig. 1](#).

The measurements were conducted using the Keysight PNA-X N5247B, and all measurements were carried out under room temperature conditions (around 300 K). The sample, positioned between the two ports, underwent S-parameter measurements. Subsequently, the acquired data was subjected to analysis through the Fresnel equation and the infinite geometric sequence. MATLAB (R2021b) was utilized for the computation, allowing the retrieval of permittivity and permeability from the S-parameters.

The signal measured is the combination of multiple reflections and transmissions so that the infinite geometric sequence can be written down.

$$\begin{cases} S_{11} = r + \frac{tr't'e^{2i\beta d}}{1 - r'^2e^{2i\beta d}} \\ S_{21} = \frac{tt'e^{2i\beta d}}{1 - r'^2e^{2i\beta d}} \end{cases} \quad (5)$$

where β is the wave number of the composite inside the waveguide of TE₀₁ mode, r, t, r', t' are the amplitude reflection and transmission coefficient.

[Fig. 2](#). illustrates the frequency dependence of complex permittivity and complex

permeability for samples with various volume fractions. When the volume fractions are below 25% in Fig. 2(a), the frequency responses across the whole bandwidth are weak. However, when the volume fractions exceed 25%, the frequency dependence becomes visible. Fig. 2(b) also has a similar trend that when the volume fraction is close to the percolation threshold, frequency response becomes apparent, as predicted in Eq. 1(b) and Eq. 2(b). We will discuss this issue in more detail later.

Fig. 3(a) is the result of ϵ' taken at 8.2 GHz (blue triangles), and 12.4 GHz (red dots). It starts from pure epoxy with a dielectric constant of around 3.03. ϵ' gradually increases from 3.2 to 8.6 as the volume fraction rises from 0% to 10%. Within this range, the silver nano-particles are isolated and can be treated as dielectric material, allowing for the application of EMT [12]. A more pronounced increase occurs at 15% to 24%, and as we further increase the volume fraction, the rate of increase (the slope) surge swiftly, and slows down when the volume fraction exceeds 25%, where the maximum relative permittivities of 515 (8.2 GHz) and 322 (12.4 GHz) were reached. The fitting result to Eq. 1(a) are given in Fig. 3(b) on a logarithmic scale. The percolation thresholds are 26.25% and 26.34%, which lie between 25.01% and 27.04%. From the fitting results, the critical exponents s are 1.3528 for 8.2 GHz and 1.2689 for 12.4 GHz, which are larger than the theoretical value. The result in this work is closer to the upper limit in two-dimensional cases, which is 1.1~1.3. The dimension of a WR90 waveguide is 22.86 mm by 10.16 mm, and the thickness chosen was 2-3mm. The shape of the samples resembles a flat slab. This might explain why the critical exponent is higher.

Fig. 4(a) shows the imaginary permittivity ϵ'' at 8.2 GHz (blue triangles) and 12.4 GHz (red dots). It has a similar trend as the real part ϵ' . A gradual increase occurs below 10%. A more pronounced rise was observed from 15% to 20% and a significant leap at 25%. Then the increasing rate slows down when raised to 27.04%, and reaches a maximum value of 716. The fitting results to Eq. 2(a) are given in Fig. 4(b) on a logarithmic scale. The percolation thresholds for the two frequencies are determined to be 26.32% and 26.39%, which also lies in the range where the increasing rate slows down. The critical exponents q are 2.2781 and 2.2840, which is lower than the theoretical value. This may cause by the prose inside the composites. Even though the authors had prevented holes on the surface, it is impossible to check whether are there prose inside without breaking the composite. The prose inside causes the imaginary part at higher volume fraction smaller than it should be, and, therefore, results in a smaller critical exponent.

According to Eq. 1(b) and Eq. 2(b) and Figs. 2(a) and 2(b), the complex permittivity is

frequency dependence near the percolation threshold. Thus, the fitting result of both ε' and ε'' to the frequency is exhibited in Fig 5. The exponents for the volume fraction of 25.01% are 0.5472 (real) and 0.6561 (imaginary), and for 27.04% are 1.0380 (real) and 1.0675 (imaginary), which is highly consistence with Eq. 1(b) and Eq. 2(b). However, the theoretical value of the frequency dependence critical exponent should be somewhere between 0 and 1[13]. The one from 27.04% is slightly higher than the theoretical value.

The permeability results are depicted in Fig. 6(a), and for ease of discussion, the negative magnetic susceptibility is also illustrated in Fig. 6(b). The difference between the two frequencies is small. At low volume fractions (<10%), the relationship between the negative susceptibility and volume fraction is quite linear, as in Fig. 6(c). Within this range, most particles remain isolated, and the cluster size remains small, making the percolation effect less apparent. Instead, the scattering model (or the effective medium theory) under the long-range approximation provides a more suitable explanation for this phenomenon.

However, as the volume fraction surpasses 15%, the impact of percolation becomes increasingly evident. The negative magnetic susceptibility increases slowly from about 0.1 to around 0.2 when the volume fraction is raised from 15% to 24%. Then, it undergoes a remarkable surge of about 0.5 at 25%, reaching a peak of approximately 0.7 at 27%.

The fitting curve of the low volume fraction range is given in Fig. 6(c). It should follow the relation [10,12]

$$-\chi_b = -N \frac{\vec{m}}{\vec{H}_{inc}} = C \cdot p_c, \quad (6)$$

where N is the number density of the silver nano-particle. The relation between the magnetic dipole and the magnetic field is $\vec{m} \sim -2S^2\vec{H}_{inc}/P$, where S is the area projected perpendicular to the field, P is its perimeter, and C is a constant.

The relation between the volume fraction and the number density is $p_c = V \cdot N$, where V is the volume of the nano-particle. For perfect spheres, $C = 2S^2/PV$ is 1.5. However, the measured slopes are 1.0375 and 1.1036 for the frequencies of 8.2 and 12.4 GHz, respectively. The obtained slopes suggest that the silver nano-particles are not ideal spheres. The value for a cubic shape is 0.5, and for any shape with approximately the same volume, the value lies between that of a sphere and a cube. Therefore, the value for an arbitrarily shaped particle should fall within the range

defined by a sphere and a cube, which aligns with our obtained result.

For the portions near the threshold, the fitting results are depicted in Fig. 6(d) on a logarithmic scale by Eq. (3). The threshold is determined to be 26.38% and 26.39%, closely aligning with the earlier obtained value. Moreover, the critical exponent u is calculated to be 0.6756 and 0.6656, which is almost twice the value of the theoretical one. However, the theoretical value in 2D is about 0.77 [10,17], which the result is closer to. The observed power law behavior of permeability in this study exhibits strong consistency with the predictions from Ref. [10].

Fig. 7(a) displays the measured imaginary permeability μ'' for two representative frequencies 8.2 and 12.4 GHz. It grew slowly and linearly when the volume fraction was increased from 2% to 10%. Then, the rate of growth paced down between 15% to 24%. As the volume fraction was further increased, the rate of increment surged swiftly to a maximum of 0.24 at 25.01%, and dropped to around 0.02 when the threshold is exceeded. The fitting result based on Eq. (4) is given in Fig. 7(b) on a logarithmic scale. The result follows the power law. The threshold is determined to be 26.60% and 25.92%, which slightly differs from the result acquired prior, but still in a reasonable region. The critical exponent v is 0.6987 and 0.6567, which is highly similar to u in 2D [10,17].

The result above shows that the prediction by Bowman and Stroud is correct for silver-epoxy composite. If we neglect the permeability (by setting it to 1), the result is given in supplementary material (Fig. SM01). The result becomes very odd. In theory, only the volume fraction near the threshold appears frequency dependency, but the frequency dependence occurs from 23.96% to 27.04% in the real part and 20.06% to 27.04% in the imaginary part., which is too wide in volume fraction. To have a better understanding, we can compare the result of $\mu = 1$ to $\mu \neq 1$, which is illustrated in supplementary material (Fig. SM02). The percolation phenomenon is less obvious, especially in the imaginary part. Also, both the real and imaginary part are smaller than the case $\mu \neq 1$. Finally, we can compare the loss tangent ($\tan \delta_\epsilon$). The loss tangent should also surge near the threshold. The loss tangent is displayed in supplementary material (Fig. SM03). It is clear that the loss tangent will surge when we consider the contribution of the permeability. This has proven that permeability plays an essential role in the EM properties of percolative metal-insulator composite. When one deals with metal-insulator composite, the effect of the permeability is not negligible.

The percolation theory sheds light on how a composite material behaves when it's near its threshold. EM properties like permittivity and permeability all show power-law dependencies.

Below the threshold, the composite is in the insulator (dielectric) phase, but there's a phase transition around the threshold that leads to the conduction phase. While there's been extensive research on the transition from insulator to conductor, percolation theory for permeability hasn't received as much attention comparatively.

The identified threshold is approximately 25.92% to 26.60%, which is relatively high [18,19]. This is due to the samples chosen. The thickness is small in comparison with the width and length, which results in the critical exponents don't show good agreement with the 3D values, instead, agree with the 2D values. The threshold in 2D problems is always higher than the 3D ones [13,14]. However, our findings align closely with the predictions made by Bowman and Stroud, particularly regarding the power-law behavior of negative susceptibility, as expressed in Eq. (3). Crucially, the results presented here hold validity across a broad bandwidth (8.2-12.4GHz). As a result of the high loss, this material can be used as stealth coating. The authors anticipate that this work will draw attention to the importance of percolation theory on complex permittivity and permeability.

REFERENCES

- [1] M. Navarro-Cía, E. Akmansoy, S. Marcellin, and J. Han, EPJ Applied Metamaterials **5** (2018).
- [2] J. B. Pendry, Phys. Rev. Lett. **85**, 3966 (2000).
- [3] T. Suzuki, M. Sekiya, T. Sato, and Y. Takebayashi, Opt Express **26**, 8314 (2018).
- [4] W. J. Padilla, D. N. Basov, and D. R. Smith, Materials Today **9**, 28 (2006).
- [5] N. Felix, L. P. Tran-Huu-Hue, L. Walker, C. Millar, and M. Lethiecq, Ultrasonics **38** (2000).
- [6] H. Y. Yao, Y. W. Lin, and T. H. Chang, Polymers **13** (2021).
- [7] S. R. Broadbent and J. M. Hammersley, Mathematical Proceedings of the Cambridge Philosophical Society. **53**, 629 (1957).
- [8] D. J. Bergman and Y. Imry, Phys. Rev. Lett. **39**, 1222 (1977).
- [9] M. A. Stephen, Phys. Lett. **87A** (1981).
- [10] D. R. Bowman and D. Stroud, Phys. Rev. Lett. **52**, 299 (1984).
- [11] A. N. Lagar'kov, L. V. Panina, and A. K. Sarychev, MRS Proceedings **232** (1991).
- [12] S. C. Su and T. H. Chang, Applied Physics Letters **116** (2020).
- [13] C. W. Nan, Prog. Mater. Sci., 1 (1993).
- [14] D. Stauffer and A. Aharony, *Introduction To Percolation Theory* (Taylor & Francis, 1992).
- [15] C. W. Nan, Y. Shen, and J. Ma, Annual Review of Materials Research **40**, 131 (2010).
- [16] C. H. Chang, S. C. Su, T. H. Chang, and C. R. Chang, Sci. Rep. **11** (2021).
- [17] A. B. Harris, Phys. Rev. B **28**, 2614 (1983).
- [18] L. Wang, Y. Bai, X. Lu, J. L. Cao, and L. J. Qiao, Sci. Rep. **5**, 7580 (2015).
- [19] K. Shehzad, A. A. Hakro, Y. Zeng, S.-H. Yao, X. H. Yi, M. Mumtaz, K. Nadeem, N. S. Khisro, and Zhi Min Dang, App. Nanosci. **5**, 969 (2015).

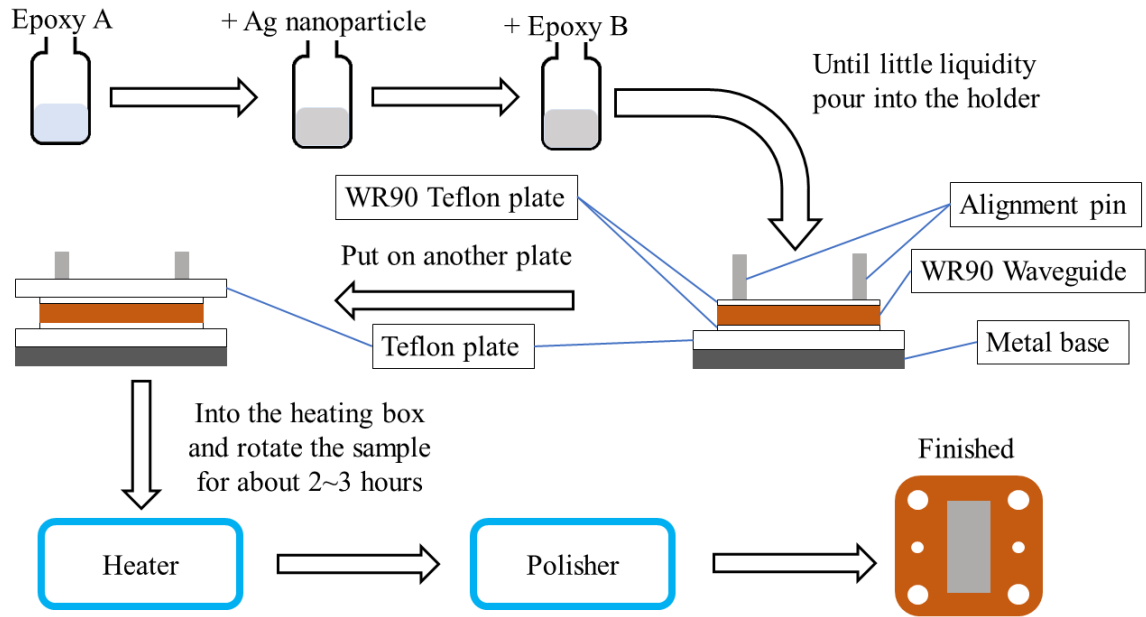


FIG. 1. The flow chart of the sample preparation for the silver-epoxy composites with a WR-90 standard rectangular waveguide.

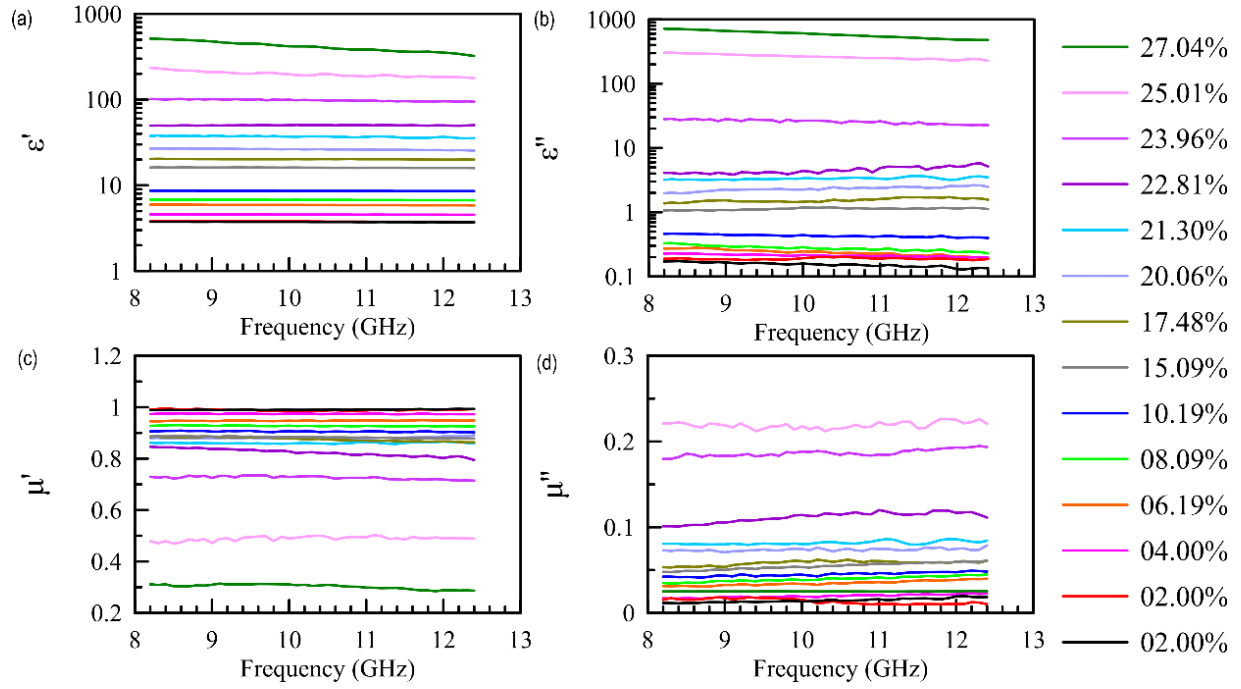


FIG. 2. The measured permittivity (a) real part and (b) imaginary part, as well as the measured permeability (c) real part and (d) imaginary part versus frequency for various volume fraction of the silver-epoxy nano-composites from 2.00% to 27.04%. Those complex permittivity and complex permeability are extracted from the measured scattering parameters based on Eq. (5).

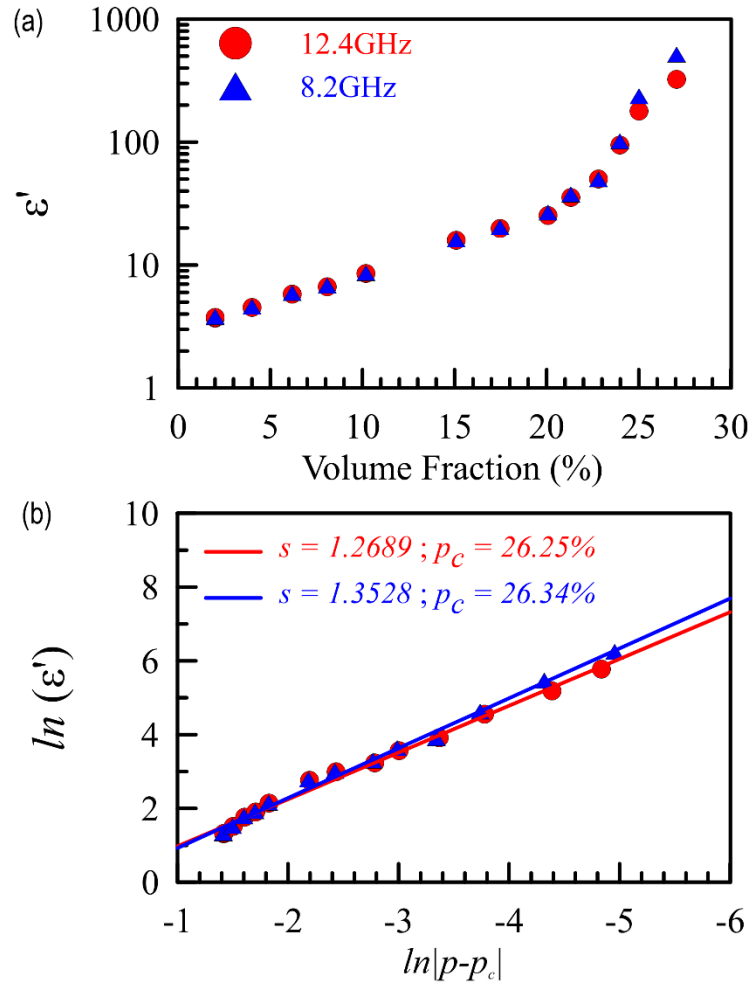


FIG. 3. (a) The measured real permittivity at 8.4 GHz (solid triangles) and 12.4 GHz (solid dots) on a logarithmic scale. (b) The fitting result to the percolation theory in Eq. (1a).

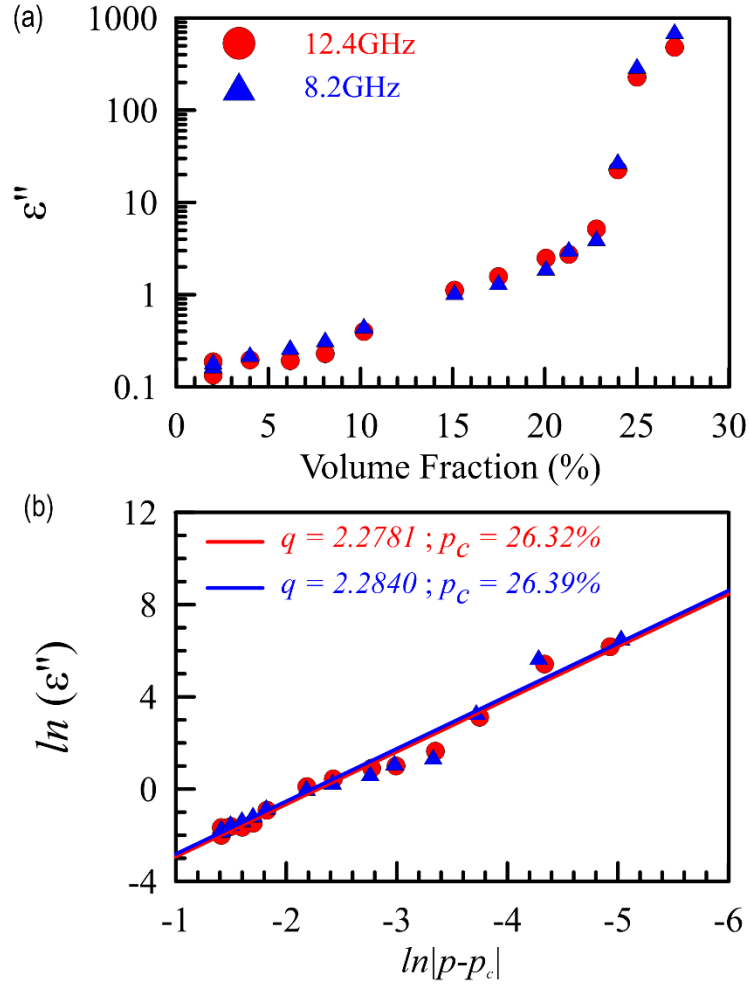


FIG. 4. (a) The result of the imaginary permittivity at 8.4 GHz (solid triangles) and 12.4 GHz (solid dots) on a logarithmic scale. (b) The fitting result to the percolation theory in Eq. (2a).

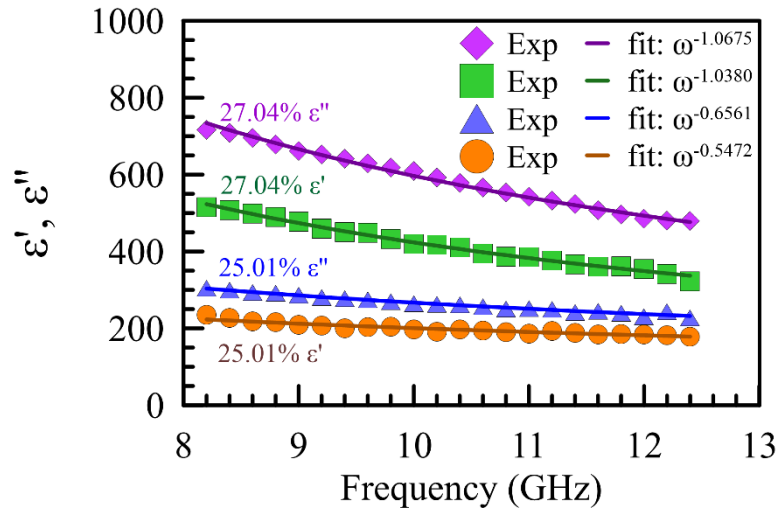


FIG. 5. The measured (solid symbols) and fitting result (solid lines) base on Eq. 1(b) and Eq. 2(b) of the frequency dependence exponent for both the real and imaginary permittivity in 25.01% and 27.04%. (27.04% ϵ'' is in purple diamonds, and ϵ' in green squares. 25.01% ϵ'' is in blue triangles, and ϵ' in orange dots.)

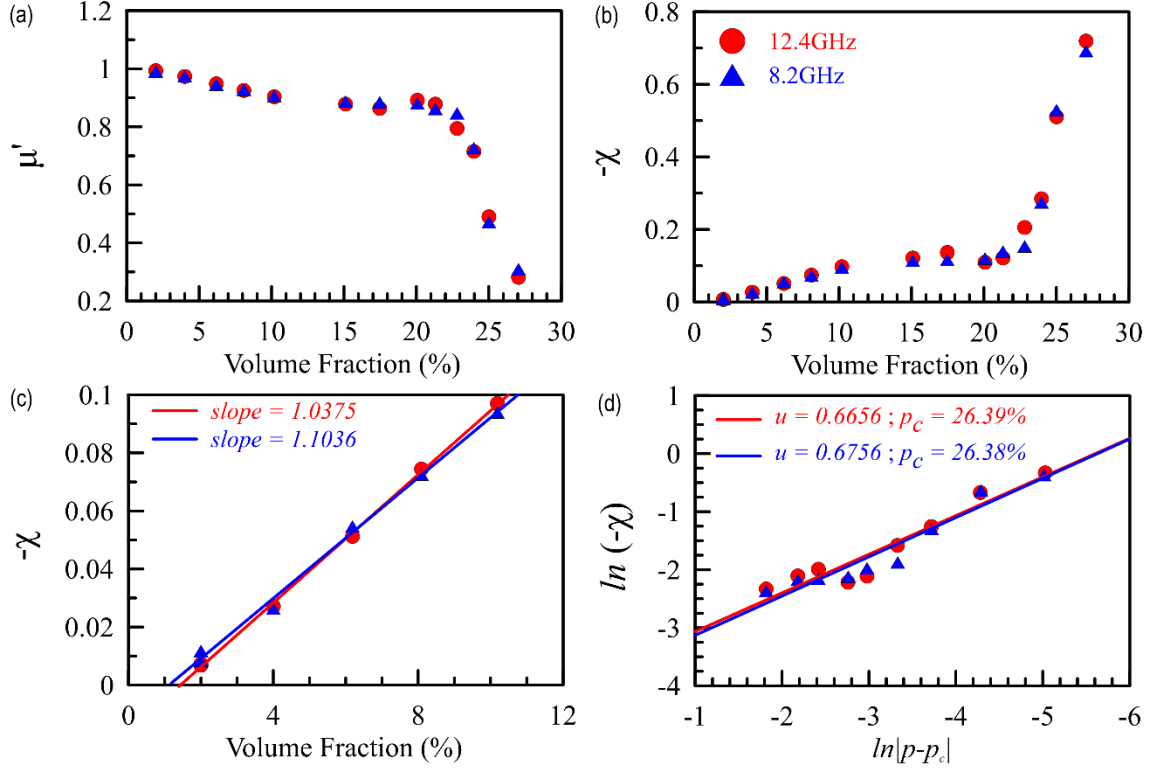


FIG. 6. The measured result (solid symbols) of the (a) real permeability and (b) negative magnetic susceptibility with respect to the volume fraction at 8.2GHz (blue) and 12.4GHz (red), and the fitting result (solid lines) in (c) the scattering region (based on Eq. (6)) and (d) the percolation region (based on Eq. (3)).

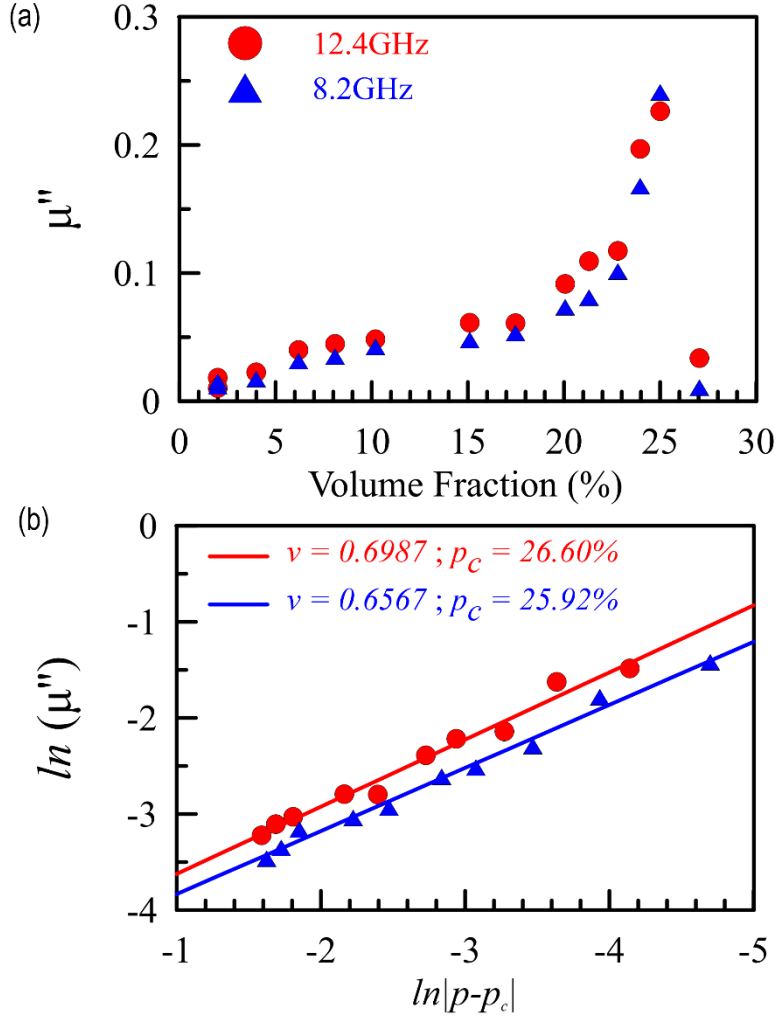


FIG. 7. (a) The result of the imaginary permeability at 8.4 GHz (solid triangles) and 12.4 GHz (solid dots) on a logarithmic scale. (b) The fitting result to the percolation theory in Eq. (4).

Percolation Effect Induced Significant Change of Complex Permittivity and Permeability for Silver-Epoxy Nano-Composites

Bo-Wei Tseng and Tsun-Hsu Chang

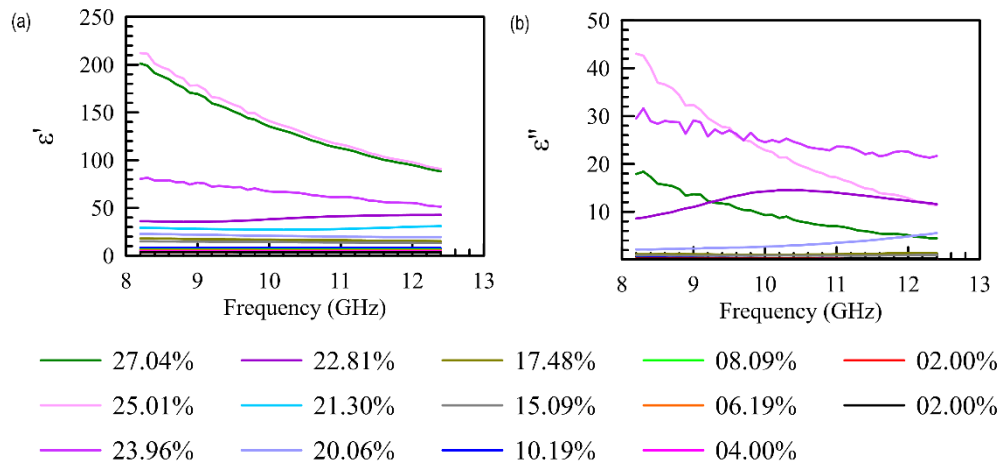


FIG. SM01. The measured permittivity (a) real part and (b) imaginary part versus frequency for various volume fraction of the silver-epoxy nano-composites from 2.00% to 27.04%. Those complex permittivities are extracted from the measured scattering parameters based on Eq. (5) by assuming $\mu=1$.

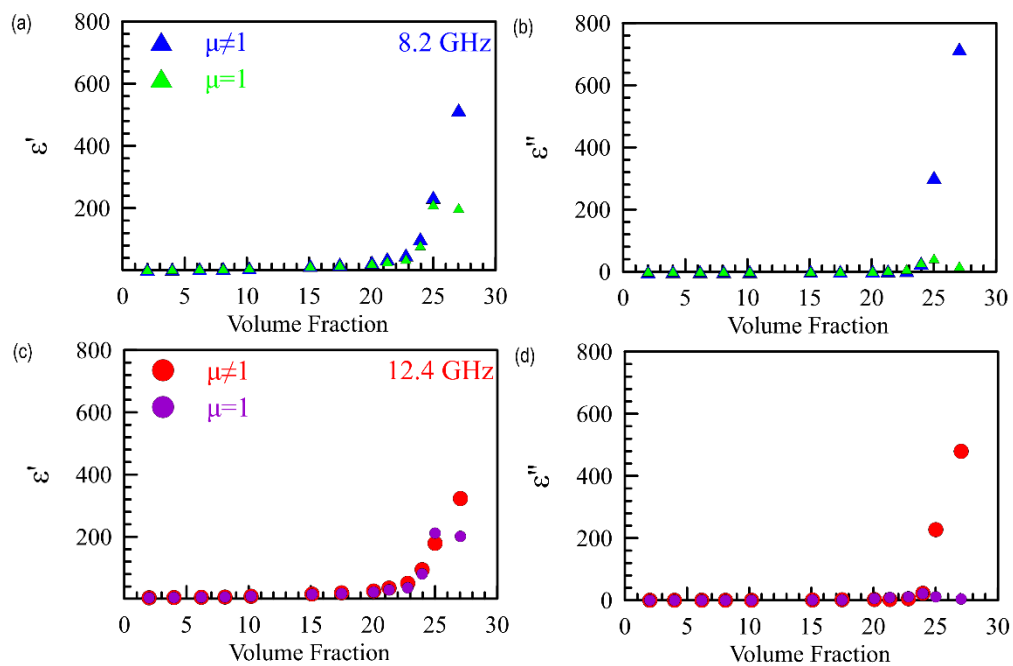


FIG. SM02. The measured (a) real permittivity and (b) imaginary permittivity at 8.4 GHz (solid triangles) as well as (c) real permittivity and (d) imaginary permittivity 12.4 GHz (solid dots) on a linear scale.

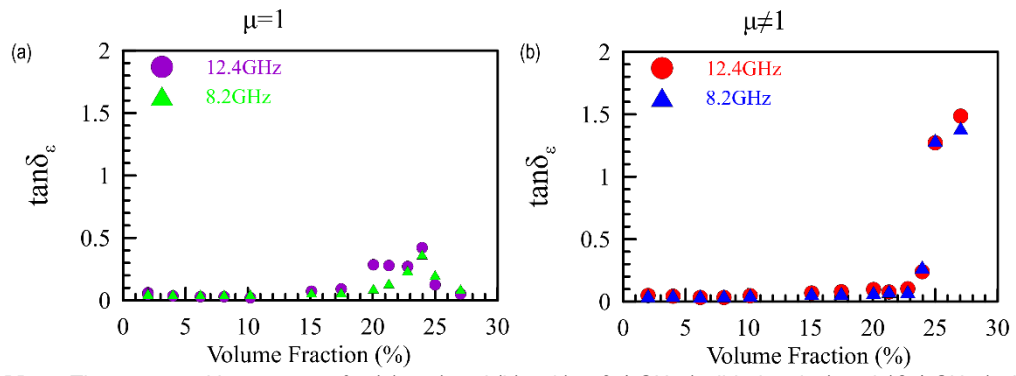


FIG. SM03. The measured loss tangent for (a) $\mu=1$ and (b) $\mu \neq 1$ at 8.4 GHz (solid triangles) and 12.4 GHz (solid dots).